J. Fluid Mech. (1987), *vol.* 177, *pp.* 233–246
Printed in Great Britain

Steady entry flow in a curved pipe

By P. H. M. BOVENDEERD, A. A. VAN STEENHOVEN, F. N. VAN DE VOSSE AND G. VOSSERS

Departments of Mechanical Engineering and Physics,
Eindhoven University of Technology, The Netherlands

(Received 28 January 1986 and in revised form 12 June 1986)

Laser-Doppler velocity measurements were performed on the entry flow in a 90° bend of circular cross-section with a curvature ratio $a/R = 1/6$. The steady entry velocity profile was parabolic, having a Reynolds number $Re = 700$, with a corresponding Dean number $\kappa = 286$. Both axial and secondary velocities were measured, enabling a detailed description of the complete flow field. The secondary flow at the entrance of the bend was measured to be directed completely towards the inner bend. Significant disturbance of the axial velocity field was not measured until a downstream distance $(aR)^{\frac{1}{2}}$. Maximum secondary velocities were measured at $1.7\,(aR)^{\frac{1}{2}}$ downstream from the inlet. The development of the axial flow field can be quite well explained from the secondary velocity field.

1. Introduction

Detailed analysis of the developing fluid flow in bends has been strongly stimulated by improved numerical and experimental methods. Moreover the subject is relevant for the understanding of blood flow in the human arterial system. A recent overview of the results of previous investigations concerning the stationary entry flow in a bend has been given by Soh & Berger (1984). Theoretical studies have been performed by Hawthorne (1951) and Smith (1976). Numerical investigations have been carried out by Singh (1974), Yao & Berger (1975), Stewartson, Cebeci & Chang (1980) and Soh & Berger (1984). Experimental analyses were made by Olson (1971), Agrawal, Talbot & Gong (1978), Choi, Talbot & Cornet (1979) and Olson & Snyder (1985). Most of these investigations deal with uniform entry flow where, immediately after the entry into the bend, a secondary flow is set up, which is dominated by the build-up of an axial boundary layer. Further downstream two helical vortices develop as a result of the interaction of inertial, centrifugal and viscous forces. The case of the development from a parabolic entry velocity profile in a situation of relative high curvature has been studied by Olson (1971). He presented only the development of the axial velocity field in the plane of symmetry of the bend.

The present study was carried out in the context of a project in which the flow pattern in the human carotid bifurcation is investigated. The blood flow in the main branch of this bifurcation, the internal carotid artery, may be partly considered as the entry flow in a bend (Olson 1971). Owing to the long straight artery between the aorta and the bifurcation the flow at the inlet of the bifurcation is assumed to be fully developed. As a first step in the investigation of the flow in the bifurcation, the steady flow development from a parabolic entry profile in a bend of relative high curvature ratio is experimentally investigated. Both axial and secondary velocity profiles, measured at several cross-sections in the bend, will be presented in this paper.

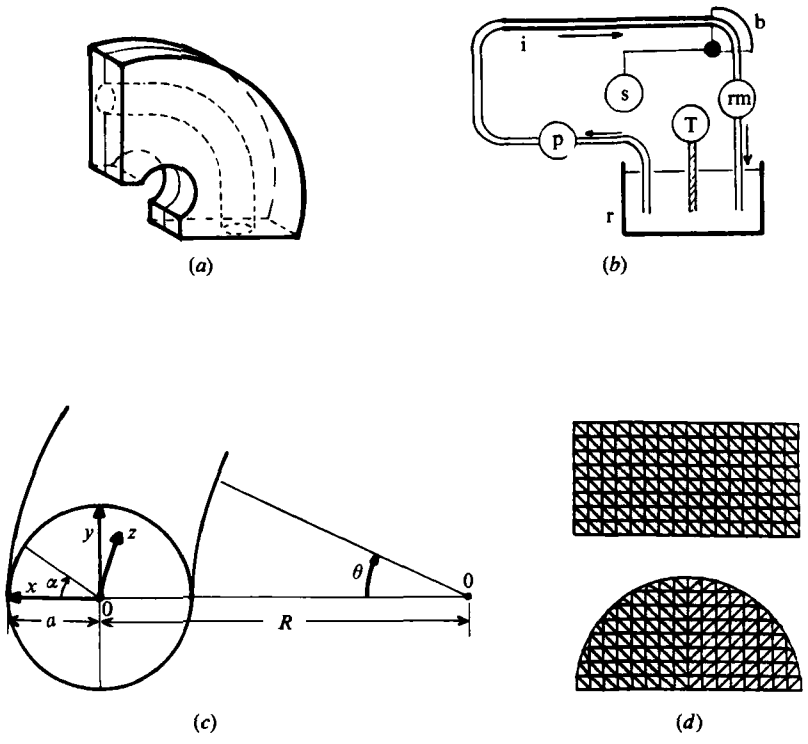

FIGURE 1. (*a*) The 90° bend. (*b*) The flow system with reservoir r, gear pump p, inlet section i, bend b, rotameter rm and temperature control T. (*c*) Coordinates in the bend. (*d*) Measuring grid and calculation grid.

2. Experimental procedure

The model in which the experiments were performed consisted of two halves of Perspex, split at the plane of symmetry, in which a 90° bend was machined out (figure 1*a*). It had an internal radius of 4.0 mm and a radius of curvature of 24.0 mm, yielding a curvature ratio $\delta = a/R$ of 1/6. The outer surfaces of the model were chosen in such a way that the three velocity components in the hereafter defined x-, y- and z-directions could be measured with the optical axis of a laser-Doppler anemometer employed perpendicular to the outer surface. The bend was placed in a flow system (figure 1*b*) in which a mixture of oil (Shellflex 214 BG) and kerosine was used as a circulating fluid. This mixture was chosen because it enabled an exact matching of the index of refraction to that of Perspex. The oil mixture was kept at a constant temperature of 40 °C in order to lower its viscosity ($\approx$ 10 cp at 40 °C) and to eliminate the influence of ambient temperature variations. Seeding with silicagel (Lichrosorb SI-100) was used to facilitate laser-Doppler measurement. The fluid was pumped out of the reservoir by a gear pump into an inlet section, consisting of a circular glass pipe of 8.0 mm internal diameter and a length of 0.4 m. This inlet section ensured a fully developed parabolic flow pattern at the entrance of the bend. Downstream of the bend there was another straight circular glass pipe, after which the fluid returned to the reservoir through a rotameter, which was used for monitoring the flow. The Reynolds number of the flow, based upon the mean axial entrance velocity W_0 and the pipe diameter $2a (Re = 2aW_0/\nu)$, was kept at 700 to within an estimated error

of 3%. This yields a corresponding Dean number $\kappa = Re\,\delta^{\frac{1}{2}} \approx 286$. The velocity components were measured by a laser-Doppler anemometer based upon the reference-beam method. A 5 mW He–Ne laser produces a laser beam which is split in two beams of equal intensity. The reference beam is led through a Bragg cell in which a frequency shift is introduced. A lens with a focal length of 80 mm intersects the two beams within the bend. The measuring volume is an ellipsoid with a length of 0.47 mm and a diameter of 0.06 mm. It could be placed at any desired location within the model by traversing the model by means of three stepper motors, enabling a smallest possible traversing distance of 0.016 mm. A photodetector measures the intensity of the light in the direction of the reference beam. The output signal of this detector is further processed by a frequency tracker (DISA 55N20) and a 12-bit analog-to-digital converter. A microcomputer controls data acquisition as well as the traversing of the model by the stepper motors and the data transfer to a mini computer (PRIME 750).

Within a cross-section perpendicular to the axis of the bend non-dimensional Cartesian coordinates $(x, y) = (x'/a, y'/a)$ are defined (figure 1*c*). The positive x-axis is directed towards the outside of the bend. The axial distance from the inlet is expressed in terms of the non-dimensional variable $z = R\theta/(aR)^{\frac{1}{2}}$, in which $(aR)^{\frac{1}{2}}$ is a characteristic distance for the development of the flow (Olson & Snyder 1983). The velocity components (v'_x, v'_y, v'_z) are made non-dimensional by dividing them by the mean entrance velocity W_0, yielding (v_x, v_y, v_z).

Velocity measurements were performed at seven axial stations in the bend: $z = 0$, 0.2, 0.5, 1.0, 1.7, 2.5 and 3.5 (corresponding to $\theta = 0$, 4.6, 11.7, 23.4, 39.8, 58.5 and 81.9°, respectively). The axial position was accurate up to an estimated error of 0.03. The velocity components were measured in a rectangular grid in one-half of the cross-section along lines parallel to the plane of symmetry. The measuring locations were situated at a distance of 1/8 from each other in both the x- and y-direction. While measuring the x- and z-component of velocity the optical axis of the anemometer was positioned perpendicular to the plane of symmetry. In this situation the measuring volume could be positioned at the first point of the grid $(x, y) = (1.0, 0)$ within an error $(\Delta x, \Delta y) = (0.0125, 0.025)$. While measuring the y-component of velocity the optical axis was situated in the x-direction, with a corresponding positioning error $(\Delta x, \Delta y)$ of $(0.025, 0.0125)$. The velocity was determined out of 20 samples of 25 μs duration each, taken over a period of 20 s. Calculation of the 95% probability intervals for axial (secondary) velocities yields an estimated error in these velocities of 1% (5%). In addition to this error the measured secondary velocity at a certain point may contain a contribution of about 2% of the corresponding axial velocity at that point, due to a possible misalignment of the plane of the laser beams and the velocity component to be measured. Furthermore some velocity smearing and averaging over the probe volume will have been present. This effect is of particular importance in regions where high velocity gradients are present, for example when measuring axial velocities near the outer wall ($\alpha = \pi$) or the x-component of secondary velocity near the upper wall ($\alpha = \frac{1}{2}\pi$). For further processing, the velocity data were converted from the measuring grid to a grid in which the pipe wall was incorporated. Measuring points within the bend were left unchanged, as shown in figure 1 (*d*). Although, owing to the extent of the measuring volume, measured velocities near the pipe wall are less reliable, these points too were maintained in the new grid. After conversion the data were finally processed into velocity profiles, isovelocity contours and vector plots.

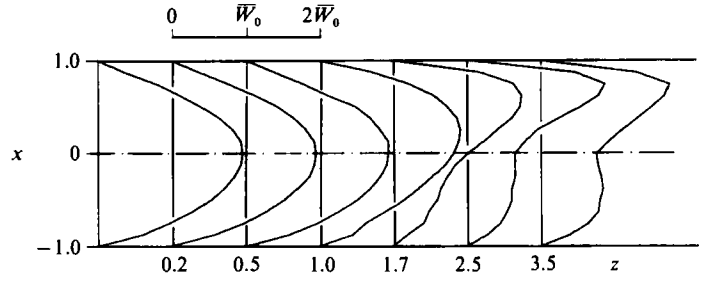

FIGURE 2. Development of the axial flow in the plane of symmetry; $\delta = 1/6, Re = 700, \kappa = 286$.

3. Results

3.1. *Axial velocities*

The development of the axial flow in the plane of symmetry is shown in figure 2. In the velocity profiles at $z = 0$, 0.2 and 0.5 hardly any influence of the curvature is visible. Further downstream the maximum of axial velocity has shifted towards the outer bend. Near the inner bend a region of relatively low axial velocity has appeared. At $z = 2.5$ this region has developed into a plateau, in which the axial velocity is approximately constant, stretching from the centre of the tube towards the inner wall up to $x \approx -0.6$. At $z = 3.5$ the plateau has disappeared again and a local minimum in the axial velocity is present at the tube centre.

A more complete picture of the axial flow development is given in figure 3, in which the flow field is represented by isovelocity contours. These contours were obtained by linear interpolation of the velocity data. The original contours are given, as smoothing may lead to loss of information. Near the tube wall the position of the contours depends heavily on the relative position of the measuring point with regard to the wall, particularly when high velocity gradients are present.

From figure 3 it is observed that the parabolic velocity profile persists at the first three axial stations, despite the clear presence of a secondary flow (which will be shown later). At $z = 1.0$ the contours have shifted towards the outer bend, becoming elliptic in shape. The axial wall shear has increased in the outer half of the bend ($-\frac{1}{2}\pi \leqslant \alpha \leqslant \frac{1}{2}\pi$), while it has decreased in the inner half. This development of the axial wall shear has continued at $z = 1.7$. The maximum of axial velocity has shifted further towards the outer wall, while a region of relative low axial velocity has appeared near the inner wall. The isovelocity contours have become C-shaped. At $z = 2.5$ the region of low axial velocity has expanded from the inner wall along the plane of symmetry towards the centre of the tube. Within a region $0 \leqslant y \leqslant 0.2$, $x \leqslant 0.2$ the axial velocity is less than 0.8. In the inner half of the bend, the isovelocity contours turn back towards the plane of symmetry. At the last station ($z = 3.5$) this process has continued: along lines parallel to the plane of symmetry double-peaked axial velocity profiles are measured up to $y \approx 0.6$. At the centre of the tube a local minimum ($v_z \leqslant 0.8$) in axial velocity has appeared, while near the inner wall the axial velocity has increased again. In the outer half of the bend the isovelocity contours are directed perpendicular to the plane of symmetry for $y \leqslant 0.4$.

3.2. *Secondary velocities*

In figure 4 (a, b) the development of the x- and y-velocity component of the secondary flow is shown. These data are combined into an overall view of the flow in figure 5.

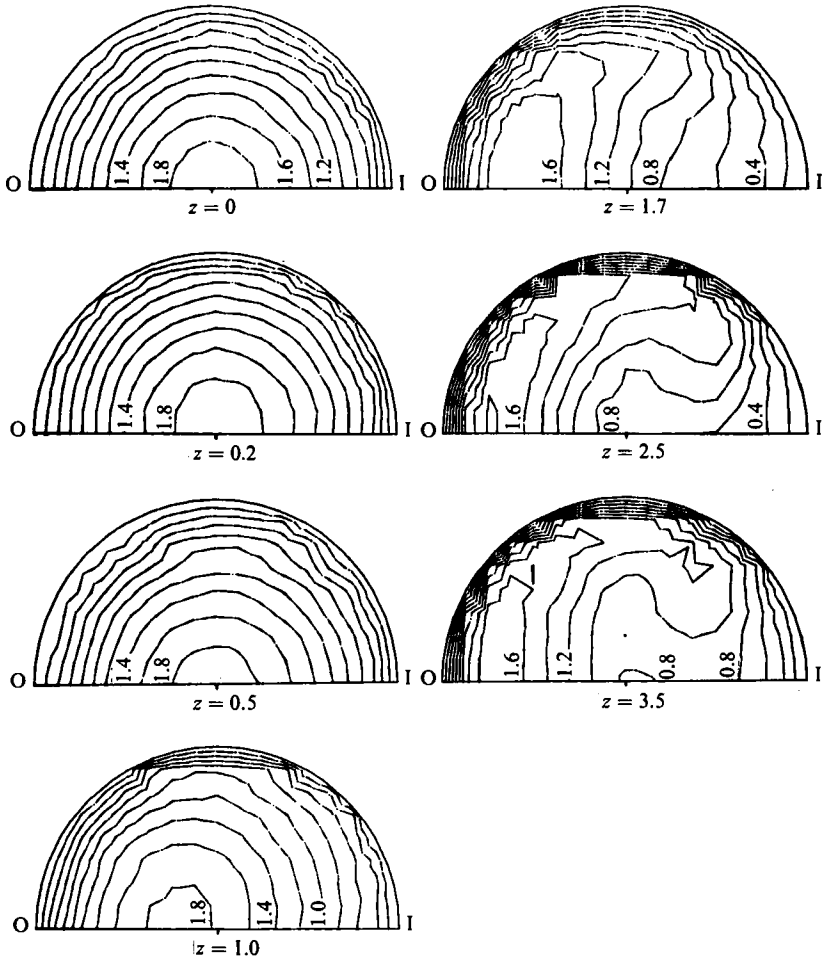

FIGURE 3. Development of the axial flow represented by isovelocity contours; $\delta = 1/6$, $Re = 700$, $\kappa = 286$; O, outer bend; I, inner bend.

At the first axial station the secondary flow is completely directed towards the inner wall. The v_x has its maximum $v_{x,\max} \approx 0.07$ along the line $x = 0$. The maximum estimated error in v_x is about 0.04 ($\approx 2\%$ of the local axial velocity) which means that, although the magnitude of v_x is quite uncertain, the measured direction of the flow is correct. The v_y differs from zero only near the inner and outer wall, where $v_{y,\max} \approx 0.025$. The point where $v_y = 0$ is situated at $x = 0$ near the upper wall, but it shifts towards the outer wall as y decreases.

At $z = 0.2$ the vector plot shows a vortex with its centre at $(x_c, y_c) \approx (0.2, 0.6)$. Near the plane of symmetry the flow is directed from the inner bend towards the outer bend. From the outer bend the fluid flows circumferentially back to the inner bend, through a layer of about $0.4a$ in width. Compared with $z = 0$ the magnitude of v_x has remained the same, but the magnitude of v_y has doubled, while maintaining its pattern. At the next axial station ($z = 0.5$) the vortex has intensified. Its centre is located at $(0, 0.65)$. The secondary flow pattern is symmetric with respect to the line $x = 0$, except for v_x in a region near the upper wall. In this layer of circumferential flow towards the inner bend, v_x reaches its maximum of 0.15 in the outer half of

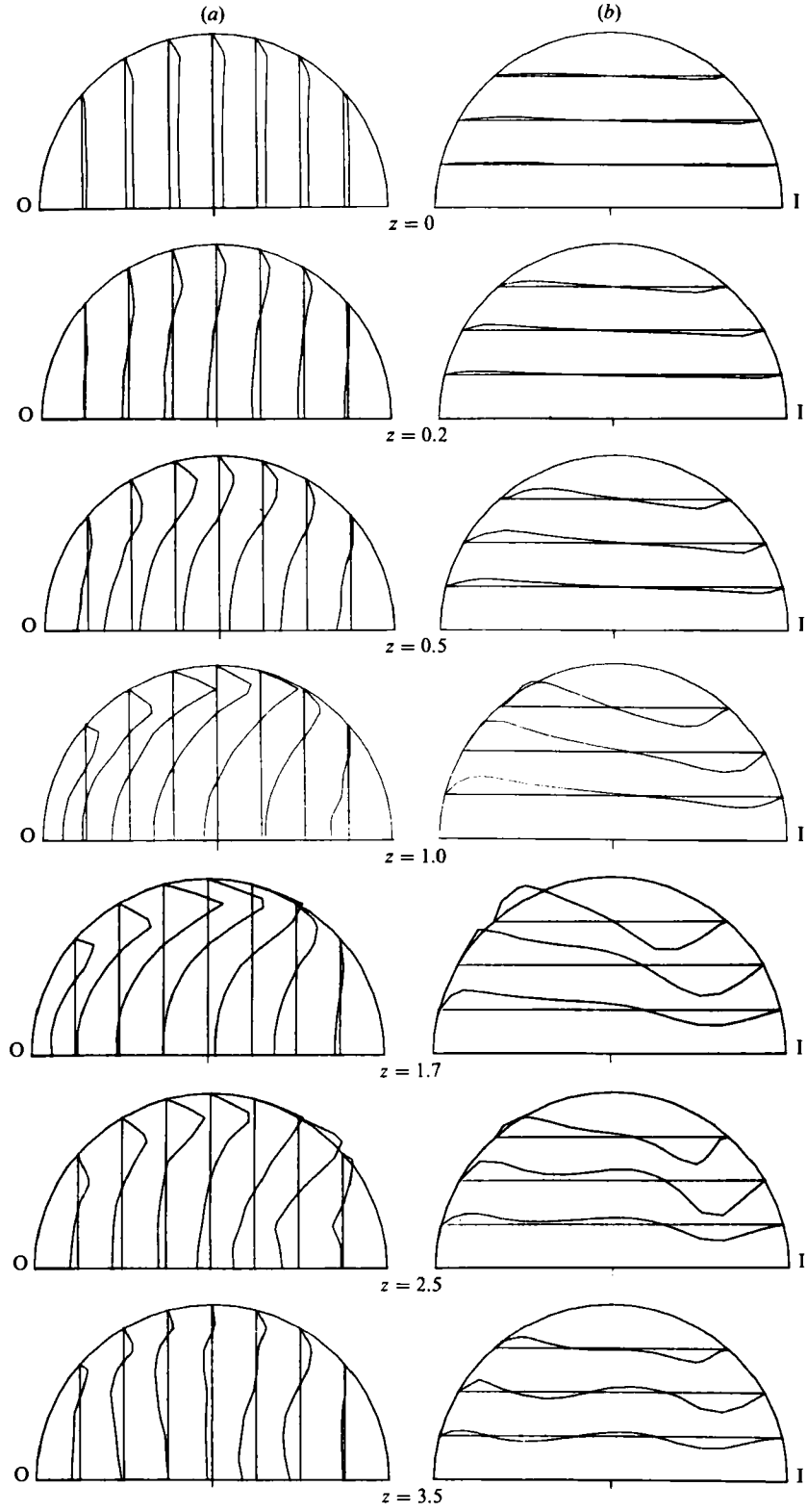

FIGURE 4. Development of the secondary flow; (*a*) x-component of secondary velocity; (*b*) y-component of secondary velocity; $\delta = 1/6, Re = 700, \kappa = 286$. The distance between two adjacent x- or y-positions, at which the profiles are given, corresponds to a velocity of $0.3W_0$.

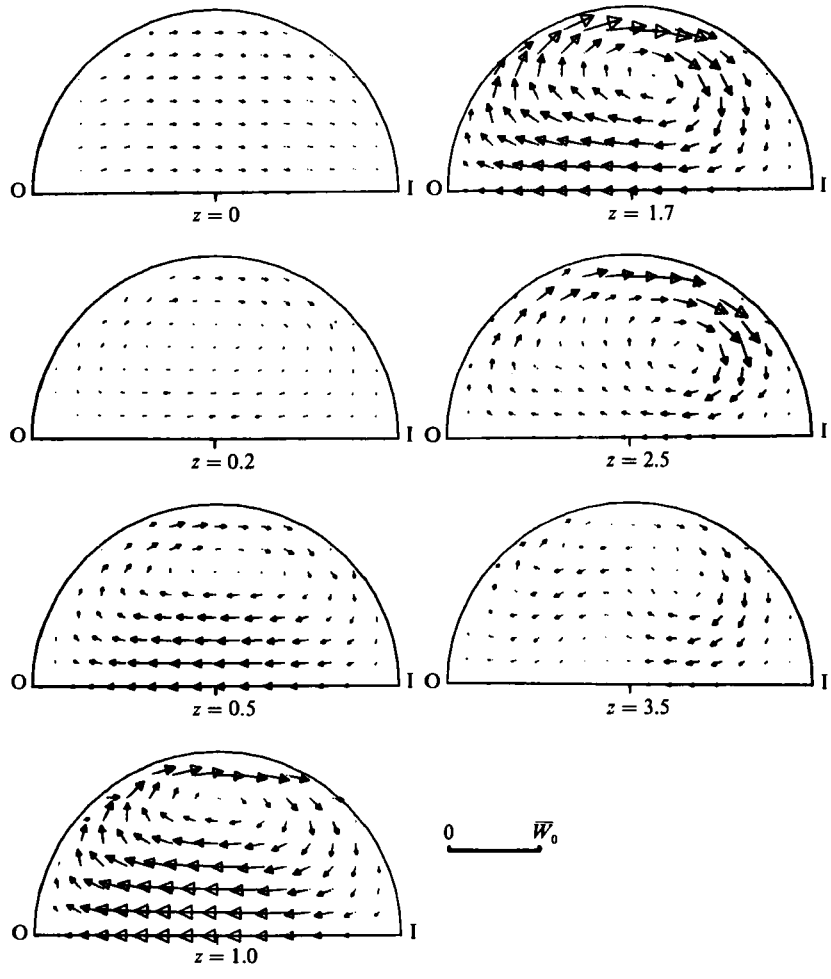

FIGURE 5. Development of the secondary flow represented by vector plots; $\delta = 1/6, Re = 700, \kappa = 286$.

the bend. The layer width has decreased to $0.3a$. Near the plane of symmetry $v_{x,\max} \approx 0.25$. The maximum v_y is measured to be 0.08.

At $z = 1.0$ the highest secondary velocities are found in the outer half of the bend. The vortex centre has moved to $(0, 0.85)$. In the plane of symmetry v_x has increased up to a maximum of 0.43. In the layer near the upper wall the maximum magnitude of v_x is 0.31. This layer of negative v_x has narrowed to approximately $0.25a$. The maximum $v_y (\approx 0.20)$ is found near the outer wall at $y = 0.5$. The line $v_y = 0$ now lies in the inner half of the bend, in contrast to the situation at $z = 0$. At the next measuring station ($z = 1.7$) the vortex centre has moved to $(0.1, 0.65)$. A decrease of v_x near the plane of symmetry ($v_{x,\max} \approx 0.31$) and an increase of this velocity component in the layer near the upper wall ($v_{x,\max} \approx 0.43$) is observed. The width of this layer has increased to about $0.4a$. At $x = -0.75$ very small values for v_x are measured. In the outer half of the bend $v_{y,\max}$ is measured to be 0.22, while in the inner half it reaches a maximum of 0.27. The region of positive v_y has expanded towards the inner bend.

At $z = 2.5$ the vortex centre lies at $(0.3, 0.45)$. The highest secondary velocities now

appear at the inner half of the bend, although the region of low secondary velocities near the plane of symmetry persists. Near the plane of symmetry v_x has decreased further. For $-1 \leqslant x \leqslant 0$ the maximum in v_x has shifted from the plane of symmetry towards the upper wall. The region of negative v_x near the upper wall has grown, particularly in the inner half of the bend. Here $v_{x,\,\max} \approx 0.33$. The v_y also reaches its maximum (0.23) near the inner bend. The v_y profiles show a dip in the outer half of the bend. At the last station ($z = 3.5$) the vortex has developed a 'tail' towards the upper wall, following the wall towards the outside of the bend. The secondary flow has sharply decreased. The circumferential flow along the upper wall has almost disappeared ($v_{x,\,\max} \approx 0.07$ here). The flow from the inner wall towards the outer wall has shifted away from the plane of symmetry, especially for $0 \leqslant x \leqslant 0.75$. For $x = 0.75$ v_x hardly differs from zero. The dip in the v_y profiles, that appeared at $z = 2.5$, now has developed into an additional region of negative v_y. The maximum $v_y\,(\approx 0.15)$ is measured in the inner half of the bend.

3.3. *Description of the flow field*

We shall now combine the results of the velocity measurements in order to give a coherent description of the flow field in the entire bend. The presence of a secondary flow at $z = 0$ indicates an upstream effect of the bend. The direction of the flow, from the inner bend towards the outer bend across the entire cross-section, is not explained yet. Neither has this effect, as far as known to us, been reported in literature. At $z = 0.2$ a vortex pattern is observed that can be explained by the interaction of inertial, centrifugal and viscous forces, as described by Berger, Talbot & Yao (1983). As the fluid enters the bend it will experience a centrifugal force because of its change in direction. This force induces a pressure-gradient force directed towards the centre of curvature. In the central core, where the axial velocities are high, the centrifugal force will dominate the pressure force resulting in an outward motion of the fluid. Near the pipe wall the situation is reversed because of the low axial velocities here; the dominating pressure force will induce a circumferential inward motion of the fluid.

Although the secondary flow has intensified at $z = 0.5$, the axial flow pattern still does not show any changes: it is apparently still dominated by inertial forces. In the axial flow pattern at $z = 1.0$ the influence of the secondary flow in the core is visible for the first time from the shift of the point of maximum axial velocity towards the outer bend. At this point the secondary flow near the plane of symmetry has reached its maximum, whereas near the pipe wall this flow increases further, as can be seen at $z = 1.7$. Here the point of maximum circumferential flow has shifted towards the inner bend. The observed deformation of the isovelocity contours might be caused by the transport of fluid by the circumferential secondary flow. Probably, the fluid with a low axial velocity, that initially found itself near the upper wall, is now situated near the inner wall. At $z = 2.5$ the axial velocity pattern has changed mainly at the inner half of the pipe, where relatively high secondary velocities are present. The secondary flow causes increasing curvature of the isovelocity contours. Moreover the secondary flow near the plane of symmetry leads to the expansion of the region of low axial velocity towards the centre of the tube. At the last axial station this region has expanded from the centre towards the upper wall. This agrees with the direction of the secondary flow. Near the inner wall the axial velocities have now increased again. Apparently the fluid that was near the pipe wall at the entrance, with a low axial velocity, has now all been swept together into the centre of the pipe. In this picture, the fluid that is now conveyed to the inner wall was originally in the

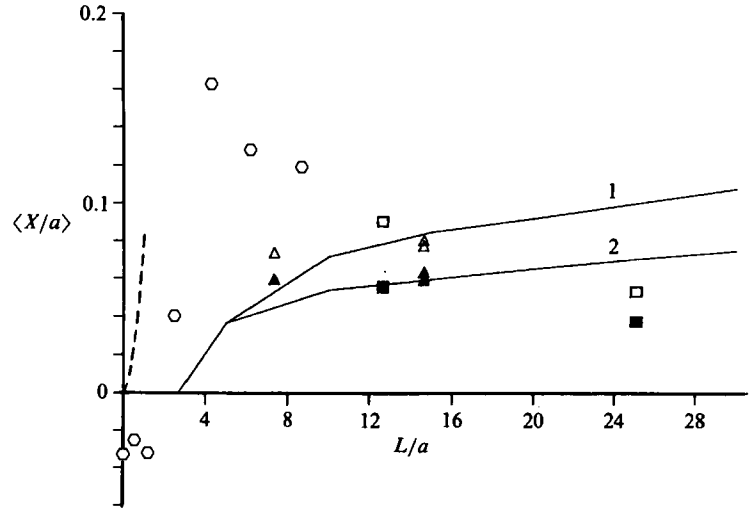

FIGURE 6. First moment of axial velocity $\langle X/a\rangle$ versus entrance length $L/a = R\theta/a$; ○, our measurements, $\delta = 1/6, Re = 700, \kappa = 286$; – – –, $\langle X/a\rangle = (\frac{1}{12}\delta)(L/a)^2$, derived from Smith (1976); Other symbols refer to data of Olson & Snyder (1985): parabolic entry profile: ▲, $\delta = 1/4.66, Re = 300$; △, $\delta = 1/4.66, Re = 1100$; ■, $\delta = 1/8.0, Re = 300$; □, $\delta = 1/8.0$, $Re = 1100$; uniform entry profile: 1, $\langle X/a\rangle$ for 'high' Re; 2, $\langle X/a\rangle$ for 'low' Re.

centre of the tube, with a high axial velocity. During the transport through the secondary boundary layer these high axial velocities have been reduced by viscous forces, but apparently this distance was too short to reduce the velocities to the velocity level of the fluid in the centre of the tube.

In the foregoing no attention has been paid to the question of whether separation of the secondary boundary layer does occur near the inner wall. Agrawal *et al.* (1978) conclude from their measurements of the x-component of secondary velocity, that separation may occur there, where a combination of a vanishing v_x near the inner wall and a shift of the maximum v_x from the plane of symmetry towards the upper wall is found. Soh & Berger (1984) suggest that separation occurs if the angle $\alpha_{\max}$, where the maximum tangential velocity is found, has shifted so close to the inner bend that the secondary flow does not have sufficient distance to turn smoothly at the inner bend, while remaining attached to the inner wall. This combination of factors does indeed apply to our measurements at $z = 1.7$, 2.5 and 3.5, with the exception of the measured v_x at $z = 2.5, x = -0.75$.

Apart from the qualitative treatment of the measurements a more quantitative description of the flow field was undertaken. For example the axial velocity profile may be quantified by its first moment $\langle X/a\rangle$, defined by Olson & Snyder (1985):

$$\langle X/a\rangle = \frac{\int_0^{\pi}\int_0^1 (v_z x)\, r\, \mathrm{d}r\, \mathrm{d}\alpha}{\int_0^{\pi}\int_0^1 v_z\, r\, \mathrm{d}r\, \mathrm{d}\alpha}, \tag{1}$$

in which $r = (x^2+y^2)^{\frac{1}{2}}$.

Figure 6 shows that $\langle X/a\rangle$ is slightly negative at the first three axial stations, after which it increases sharply up to a maximum value $\langle X/a\rangle \approx 0.16$ at $z = 1.7$. This indicates a shift of the axial flow towards the inner bend for $z \leqslant 0.5$, which agrees with the measured direction of the secondary flow at $z = 0$. The shift of axial flow

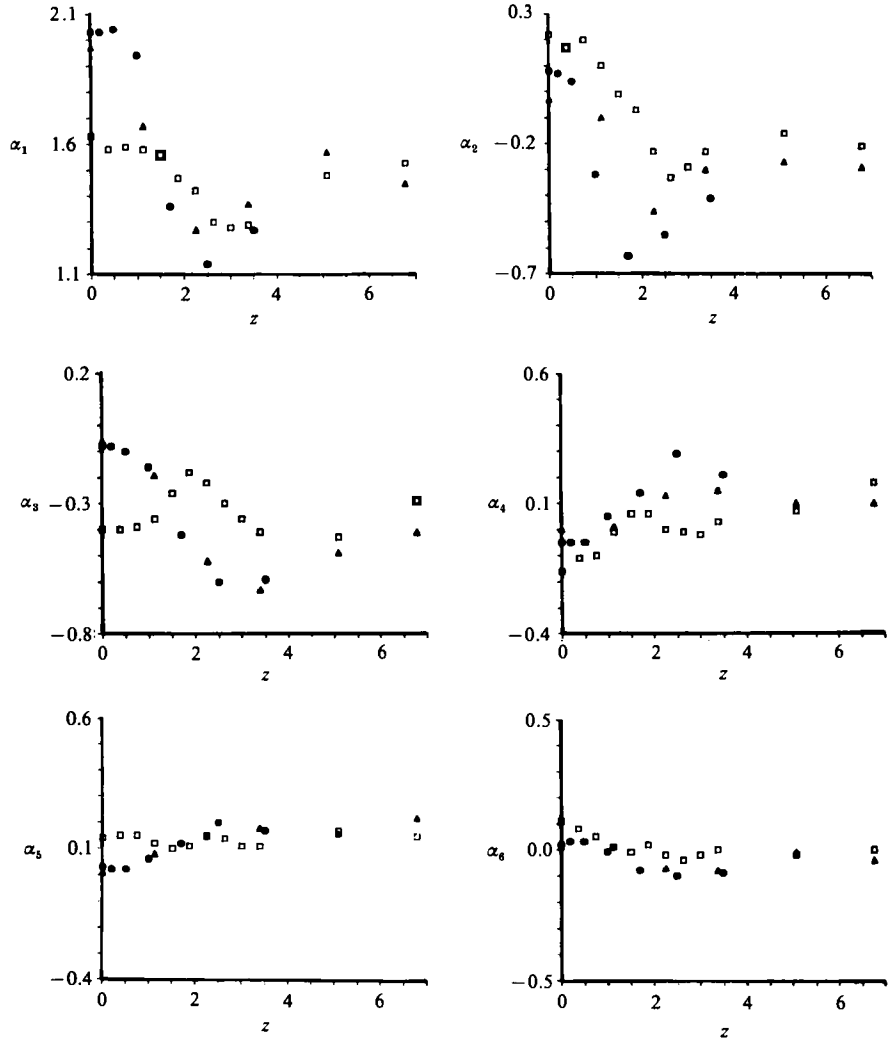

FIGURE 7. Coefficients α_i when developing the axial velocity field in the plane of symmetry into a Fourier series. ●, our measurements, $\delta = 1/6, Re = 700, \kappa = 286$; parabolic (▲)- and uniform (□)-entry-profile values derived from Olson (1971) for $\delta = 1/4.66, Re = 540, \kappa = 250$.

towards the inner bend is followed by an overshoot towards the outer bend at $z = 1.7$. Olson & Snyder conclude that $\langle X/a \rangle$ develops on an axial scale a for both uniform and parabolic inlet profiles. In the uniform-entry case they find a monotonic increase of $\langle X/a \rangle$ for increasing L/a, in contrast to the situation for a parabolic entry profile. There is some qualitative agreement between our results and Olson & Snyder's data for a parabolic entry profile, although in our case the maximum $\langle X/a \rangle$ is larger and reached earlier.

Another way of quantifying the axial flow field lies in developing the axial velocity profile in the plane of symmetry $v_z(x)$ into a Fourier series:

$$v_z(x) = \sum_{1}^{N} \alpha_i f_i(x). \tag{2}$$

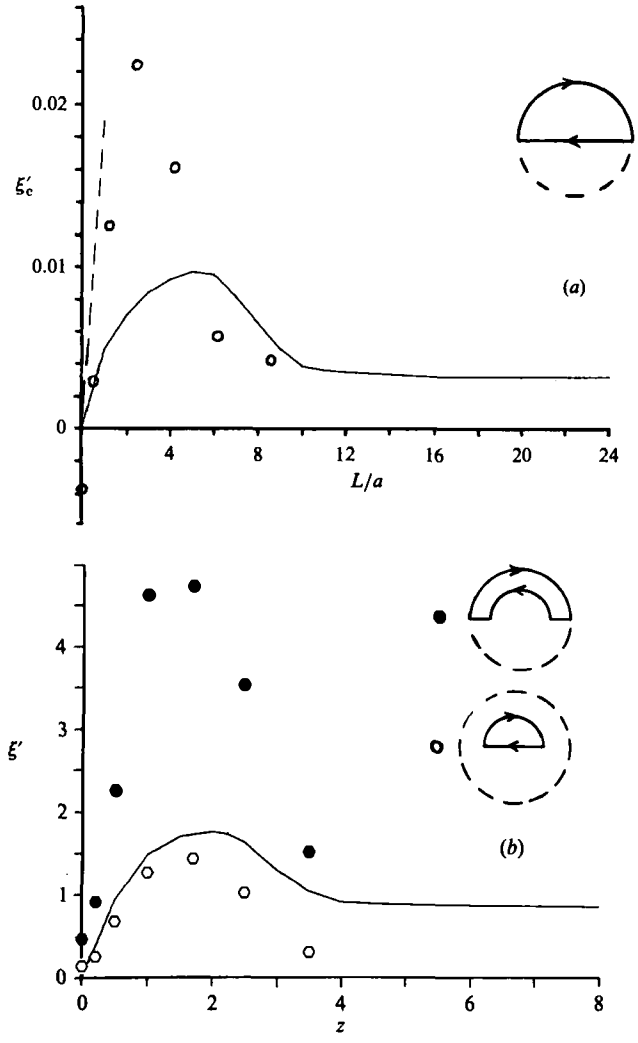

FIGURE 8. Development of the mean axial vorticity: (*a*) in central core: $\xi'_c = \xi_c \delta^{\frac{3}{2}}$: ○, our measurements, $\delta = 1/6, Re = 700, \kappa = 286$; ---, $\xi_c = (16/3\pi)\delta(L/a)$ derived from Smith (1976); ——, general development for 'low' κ (Olson & Snyder 1985). (*b*) on maximum circulation path: $\xi' = \xi(Re)^{\frac{1}{3}}$: ξ_{max}(○) and ξ_{bl}(●) as calculated from our measurements; ——, general development of ξ_{max} (Olson & Snyder 1985).

The Fourier functions for $-1 \leqslant x \leqslant 1$, being zero at $x = 1, x = -1$, are defined as

$$\left.\begin{aligned} f_{2n+1}(x) &= \cos(\tfrac{1}{2}(2n+1))\pi x, \quad n = 0, 1, \ldots, \\ f_{2n}(x) &= \sin(n\pi x), \qquad\qquad n = 1, 2, \ldots, \end{aligned}\right\} \tag{3}$$

The approximation by a series up to the 6th degree already gave a reasonable fit: the standard deviation reached a maximum of 0.088 for the profile at $z = 2.5$. The coefficients α_i are displayed in figure 7. This figure also shows data derived from Olson (1971) for a parabolic and a uniform entry profile. Our data agree quite well with Olson's data for a parabolic entry profile, whereas the main differences with the uniform entry profile appear in α_1 and α_3.

Finally, the secondary flow field is quantified by its mean axial vorticity ξ, defined as (Olson & Snyder 1985)

$$\xi = \frac{\Gamma}{A} = \frac{1}{A}\oint_S \boldsymbol{v}\cdot\mathrm{d}\boldsymbol{s}, \tag{4}$$

where S is taken in a plane of constant z, surrounding a region with surface A. Taking S along the plane of symmetry and the upper pipe wall we find the vorticity ξ_c in the central core. In fact ξ_c quantifies the x-velocities in the plane of symmetry. Figure 8(a) shows that in our case with a parabolic entry profile the maximum ξ_c is larger and reached earlier than in Olson's case with a uniform entry profile. The decrease of ξ_c at the last two axial stations is primarily caused by the decrease of the total secondary flow. Further downstream the additional effect of the shift of the maximum velocity in the x-direction away from the plane of symmetry plays a role. In figure 8(b) the vorticity on a path of maximum circulation is presented. The quantity ξ_{max} was calculated along a path S consisting of a semicircle in the upper half of the bend, closing the loop along the plane of symmetry. The maximum vorticity in the boundary layer ξ_{bl} was also calculated along a semicircle, but here the loop was completed along the pipe wall. In both cases maximum circulation Γ was found by varying the radius of the semicircle. According to Olson & Snyder (1985) these quantities are best correlated by a lengthscale $(aR)^{\frac{1}{2}}$. ξ_{max} and ξ_{bl} appear to be closely coupled, ξ_{bl} being about three times as large as ξ_{max}. While maximum ξ_c was found at $z = 1.0$, in this case maximum vorticities are found at $z = 1.7$. The latter corresponds well with the general finding of Olson & Snyder (1983, 1985) that maximum vorticity occurs at $z \approx 2$. The sharp decrease of vorticity for $z > 2$ in our measurements is probably caused by the straight pipe following the bend at $\theta = 90°$.

4. Discussion

In the present paper a detailed description is given of the axial and secondary fluid velocities in a 90° bend, with a high curvature ratio and a parabolic entry profile. Although the effect of curvature is hardly visible in the isovelocity contours at $z = 0$, 0.2 and 0.5, the first moment of axial velocity $\langle X/a \rangle$ reveals an inward shift of the axial velocity field in the entrance region. The measured secondary flow at $z = 0$ was directed towards the inner bend across the entire cross-section. Both these effects indicate an upstream effect of the curvature. The development of the axial flow field for $z \geqslant 1.0$, showing the C-shaped isovelocity contours that have also been observed by other investigators (for example Agrawal *et al.* 1978 and Olson & Snyder 1985), is quite well explained from the shape of the secondary velocity field. The basic vortex shape of the secondary flow field, measured for $z \geqslant 0.2$, can be explained from the interaction of inertial, centrifugal and viscous forces. A more detailed view of this vortex reveals features that are not yet explained, like the shift of the vortex centre and the development of a 'tail'.

Our results may be compared with the theoretical results of Smith (1976), who studied the flow development in a straight pipe followed by a curved pipe at $z = 0$. Applying perturbation theory of $O(\delta)$ to the oncoming flow, Smith finds no disturbance of the inviscid core for $z < 0$. In the boundary layer however, an upstream response is found, showing a rise of pressure near the outer bend ($\alpha = 0$) and a pressure fall at the inner bend ($\alpha = \pi$), inducing a secondary flow towards the inner bend and an increase of axial shear at that position. We find an upstream

response too, although in our measurements the secondary flow towards the inner bend stretch over the entire cross-section.

For $R\theta/a = O(1)$ Smith does find a perturbation of the core flow, which applied to our situation with a parabolic entry profile and $\delta = 1/6$ yields ($z = O(\delta^{\frac{1}{2}})$)

$$\left.\begin{aligned} v_x &= 2\delta^{\frac{1}{2}}z(1-r^2), \\ v_y &= 0, \\ v_z &= 2(1-r^2)+2xz^2. \end{aligned}\right\} \tag{5}$$

The relationship for v_x shows an $(1-r^2)$-dependence, which is also observed in our measurements. The magnitude of v_x is overestimated by (5), as is apparent also from the values of ξ_c, calculated from (5) for $-1 \leqslant x \leqslant 1$ and given in figure 8(*a*). The z-dependence cannot be checked from our measurements. In his $O(\delta)$-solution Smith finds no v_y in the core, whereas we measure a v_y that is very much smaller than the v_x disturbance. The secondary flow towards the outer bend causes axial shear stress to rise there, and a crossover of maximum axial shear towards the outer bend is found by Smith at a downstream distance $R\theta/a = 1.51, z \approx 0.62$, which is in agreement with our findings. The perturbation of the axial velocity field results in a first moment $\langle X/a \rangle$, calculated over $0 \leqslant r \leqslant 1$, being positive and proportional to z^2, as shown in figure 6. This does not agree with our observation of an inward shift of the axial velocity field. The secondary flow in the boundary layer is directed azimuthally towards the inner bend, thus completing the familiar vortex pattern.

Other analyses, available from literature, of the steady laminar entry flow in a curved tube of relative high curvature ratio almost always deal with uniform entry flow. Bearing in mind the difference in entry velocity profile, our results may be compared with the experimental uniform-entry-profile results of Agrawal *et al.* (1978) for $\delta = \frac{1}{8}, Re = 365, \kappa = 183$, and Olson & Snyder (1985) for $\delta = \frac{1}{8}$, $Re = 1100, \kappa = 390$. The calculated uniform-entry-profile results of Soh & Berger (1984) for $\delta = \frac{1}{7}, Re = 484, \kappa = 183$, will also be used for comparison. In the axial flow field in the uniform-entry case a shift of the maximum axial velocity towards the inner bend is observed for $z \leqslant 1.5$, in contrast to the situation with a parabolic entry flow. Further downstream this maximum shifts towards the outer bend, although for $z \leqslant 3.5$ the differences between the two entry cases are still considerable. The secondary flow with a uniform entry profile is more or less dominated by the build-up of an axial boundary layer, appearing from a radial inward secondary motion. This pattern occurs for $z \leqslant 0.5$. Further downstream both entry-profile cases show approximately the same secondary flow pattern. For $z = 1.0$ in our results the v_x appears to be larger in the central core than near the upper wall, while in the uniform-entry case the situation is reversed. For $z = 1.7$ and 2.5 the results in both entry-flow cases agree quite well, although Agrawal finds a secondary boundary layer near the upper wall that is quite thin compared with the other results. At $z = 3.5$ we find relatively small secondary velocities, compared with results from literature. Probably this is caused by the upstream effect of the straight pipe following the bend at $\theta = 90°$. The shape of the vortex, showing a tail towards the outer bend, is quite different from the shape Soh & Berger find for $\delta = \frac{1}{7}, \kappa = 183$. In fact it does agree better with the vortex that they compute for $\delta = \frac{1}{7}, \kappa = 680$.

The results of the various investigations are also compared by quantitative analyses. Olson & Snyder (1985) use the first moment $\langle X/a \rangle$ to quantify the axial flow, whereas in this paper the Fourier analysis of the axial velocity profile in the plane of symmetry is introduced. The observed differences between our and Olson's

data with regard to the first moment are remarkable and as yet unexplained, but the agreement between the Fourier coefficients of the axial velocity profiles in the plane of symmetry is quite satisfactory. Besides, the mean axial vorticity ξ in each cross-section, introduced by Olson & Snyder (1985) to characterize the secondary flow field, shows a good resemblance with our data.

We wish to thank Ir J. A. W. M. Corver for his support in the initial phase of this study and Mr J. W. G. Cauwenberg for his technical assistance.

REFERENCES

AGRAWAL, Y., TALBOT, L. & GONG, K. 1978 Laser anemometer study of flow development in curved circular pipes. *J. Fluid Mech.* **85**, 497–518.

BERGER, S. A., TALBOT, L. & YAO, L. S. 1983 Flow in curved pipes. *Ann. Rev. Fluid Mech.* **15**, 461–512.

CHOI, U. S., TALBOT, L. & CORNET, I. 1978 Experimental study of wall shear rates in the entry region of a curved tube. *J. Fluid Mech.* **93**, 465–489.

HAWTHORNE, W. R. 1951 Secondary circulation in fluid flow. *Proc. R. Soc. Lond.* A **206**, 374–387.

OLSON, D. E. 1971 Fluid mechanics relevant to respiration: flow within curved or elliptical tubes and bifurcating systems. Ph.D. thesis, University of London.

OLSON, D. E. & SNYDER, B. 1983 The growth of swirl in curved circular pipes. *Phys. Fluids* **56**, 347–349.

OLSON, D. E. & SNYDER, B. 1985 The upstream scale of flow development in curved circular pipes. *J. Fluid Mech.* **150**, 139–158.

SINGH, M. P. 1974 Entry flow in curved pipe. *J. Fluid Mech.* **65**, 517–539.

SMITH, F. T. 1976 Fluid flow into a curved pipe. *Proc. R. Soc. Lond.* A **351**, 71–87.

SOH, W. Y. & BERGER, S. A. 1984 Laminar entrance flow in a curved tube. *J. Fluid Mech.* **148**, 109–135.

STEWARTSON, K., CEBECI, T. & CHANG, K. C. 1980 A boundary-layer collision in a curved duct. *Q. J. Mech. Appl. Maths* **33**, 59–75.

YAO, L. S. & BERGER, S. A. 1975 Entry flow in a curved pipe. *J. Fluid Mech.* **67**, 177–196.